Quaternary Science Reviews 245 (2020) 106461

Contents lists available at ScienceDirect

Quaternary Science Reviews

journal homepage: www.elsevier.com/locate/quascirev

Late Glacial mountain glacier culmination in Arctic Norway prior to the Younger Dryas

Hella E. Wittmeier [a, b], Joerg M. Schaefer [c, d, *], Jostein Bakke [a, b], Summer Rupper [e], Øyvind Paasche [b], Roseanne Schwartz [c], Robert C. Finkel [f]

[a] Department of Earth Science, University of Bergen, Allégaten 41, N-5007, Bergen, Norway
[b] Bjerknes Center for Climate Research, Allégaten 41, N-5007, Bergen, Norway
[c] Lamont-Doherty Earth Observatory, Geochemistry, Palisades, NY 10964, USA
[d] Department of Earth and Environmental Sciences, Columbia University, New York, NY 10027, USA
[e] Department of Geography, University of Utah, 260 S Central Campus Dr., Salt Lake City, UT 84112, USA
[f] University of California, Berkeley, Department of Earth and Planetary Sciences, Berkeley, CA 95064, USA

ARTICLE INFO

Article history:
Received 23 February 2020
Received in revised form
16 June 2020
Accepted 26 June 2020
Available online 12 August 2020

Keywords:
Glaciation
Paleoclimatology
Pleistocene
North Atlantic
Cosmogenic isotopes

ABSTRACT

Climate changes during the Late Glacial period (LG; 15-11 ka) as recorded in Greenland and Antarctic ice cores show a bipolar pattern. Between 14.5 ka and 13 ka ago, the northern latitudes experienced the Bølling/Allerød (BA) warm period, while southern records feature the Antarctic Cold Reversal (ACR). Between 12.9 ka and 11.7 ka ago, the north was under the Younger Dryas (YD) cold spell while southern latitude temperature rose in parallel to atmospheric CO2 concentrations. While the southern hemisphere pattern is well documented in mountain glacier moraine records from New Zealand and Patagonia, in northern mid-latitudes and the Arctic, the LG glacier culmination has been connected to the YD stadial, apparently confirming the bipolar pattern.

We present a geomorphic map of mountain glaciers in Arctic Norway, a cosmogenic nuclide chronology from 71 moraine boulders from the LG and the Holocene, and first-order glacier modeling experiments. The model and dating results show that the studied mountain glaciers are most sensitive to summer-temperature change, that their response to those changes is highly correlated to a wider region and that these mountain glaciers in Arctic Norway reached their maximum LG extent about 14 ka ago, prior to the YD. Following considerable retreat through the first part of the YD, glaciers re-stabilized in the mid-YD and showed slower oscillatory retreat through the latter part of the YD. We compare this glacier pattern to updated earlier glacier records in the wider Arctic and North Atlantic region and propose a pattern of coherent glacier response to climate changes during this interval.

The LG results from Arctic glaciers show consistency to the glacier record from New Zealand and Patagonia. This first-order interhemispheric coherency of LG mountain glacier fluctuations driven mainly by summer temperature would support the view that the bipolar seesaw was primarily a northern winter phenomenon during the LG period, and the YD in particular. More similar experiments need to be performed to further test this scenario.

1. Introduction

Mountain Glaciers are sensitive to changing climate (Oerlemans, 2001, 2005), and outside arid regions, summer temperature change dominates the glacier mass balance (Rupper and Roe, 2008). During the LG period (15-11 ka), the atmospheric temperature and greenhouse gas concentrations completed the transition from the last ice age to the ongoing inter-glacial, the Holocene (last 11,600 years). But the LG temperature patterns and the Atlantic ocean overturning strength between the hemispheres were antiphased, dubbed a bipolar seesaw (Broecker, 1998). In Scandinavia and Europe, the moraines deposited during the LG glacier culmination have been connected to the YD stadial (Aarseth and Mangerud, 1974; Andersen et al., 1995; Goehring et al., 2012; Ivy-Ochs et al., 2009; Rasmussen et al., 2006). In Arctic Norway, mountain

* Corresponding author. Lamont-Doherty Earth Observatory, Geochemistry, Palisades, NY 10964, USA.
E-mail address: schaefer@ldeo.columbia.edu (J.M. Schaefer).

https://doi.org/10.1016/j.quascirev.2020.106461

glaciers developed after the Scandinavian Ice Sheet (SIS) had retreated over the region around 15.7 ka (Stokes et al., 2014). These mountain glaciers subsequently deposited characteristic moraine sequences in the coastal areas of Nordland, Troms and Finnmark (Andersen, 1968; Kverndal and Sollid, 1993; Sollid et al., 1973). Traditionally, LG SIS culminations in Norway have also been linked to the YD stadial (Andersen et al., 1995; Goehring et al., 2012). As a result, many LG landforms in Arctic Norway are referred to as 'Younger Dryas moraines', while questions remain about the timing of these mountain glacier events through the LG period (Andersen et al., 1995; Bakke et al., 2005; Evans et al., 2002; Paasche et al., 2007; Romundset et al., 2011; Wittmeier et al., 2015). A recent study postulated the demise of the Scotland Ice Sheet through the YD period, driven by warming summer temperatures (Bromley et al., 2014); a finding that seems hard to reconcile with the existing chronologies of LG mountain glacier culminations in Scandinavia and the Alps. We here present a detailed reconstruction of mountain glacier fluctuations on the Island of Arnøya in Arctic Norway throughout the LG and Holocene. Our study combines comprehensive geomorphologic mapping, ^{10}Be exposure dating of 71 boulders from thirteen moraines and a first-order glacier modeling study (Supplementary Information) to evaluate the amplitudes of the climate changes most likely related to the observed glacier changes. First, we compare our results from Arctic Norway with updated existing chronologies from southwest Norway (Briner et al., 2014; Mangerud et al., 2013) and Greenland (Kelly et al., 2008; Levy et al., 2016) to develop a regional North Atlantic region perspective of glacier and summer temperature change. We then test for any inter-hemispheric patterns by comparing our new chronology with existing studies of similar detail from southern mid-latitudes.

2. Setting

We focus on the Rødhetta Glacier moraine record, complemented by data from the neighboring Nymoen Glacier and Snøfonn snow-field (Fig. 1). Rødhetta and Nymoen Glaciers are relatively simple mountain glaciers that were land-terminating during their maximum LG extent (see 2.1.) and ever since. The Rødhetta moraine record displays striking similarity to other moraine sequences on the Island of Arnøya (Kverndal and Sollid, 1993), the Bergsfjord Peninsula (Wittmeier et al., 2015), the Lyngen Peninsula (Bakke et al., 2005) and the Island of Andøya (Møller and Sollid, 1972; Paasche et al., 2007), illustrating the regional relevance of the glacier and climate changes reflected in the studied moraine record. On the regional scale, our climate correlation maps shown in Fig. 2 illustrates the high spatial correlation of the Rødhetta glacier location with the climate across Europe and bordering regions in general. Please note the particularly high correlation with the Arctic-Eurasian summer temperature, throughout Scandinavia, the Baltics, western Russia and the Alps, shown in the left panel of Fig. 2.

2.1. Geological setting

The Island of Arnøya (70°08′ N 20°35′ E) covers 276 km^2 with alpine peaks reaching nearly 1200 m altitude intersected by wide glacially carved valleys, large scree slopes, rock glaciers and numerous cirques. The present climate of Arnøya is maritime due to its location at the eastern rim of the northern North Atlantic Ocean. A mean (1961–1990) summer (May to September) temperature of 8.7 °C is measured at the climate station No. 92700 Loppa (10 m a.s.l.), ~40 km north-northeast from the study site. The mean temperature in July is 11.6 °C. The mean winter (October to April) temperature for the same period is 0 °C, and the mean annual temperature is 3.6 °C. The mean measured winter precipitation is 560 mm for the 1961–1990 period, and the mean annual precipitation is 914 mm (MET station ARNØYA - TROLLTINDEN 91729 http://eklima.met.no/Help/Stations/toDay/all/en_e91729.html; February 2020). The bedrock is allochthonous metamorphic bedrock of Cambrian age (Roberts, 1973). In the catchment area of Rødhetta glacier, the bedrock lithology shows alternating layers of garnet and amphibolite, partly granitized, fine- to medium-coarse gneiss with layers of limestone, and greenstone, green shale and amphibolite.

The boulders sampled in this study display traversing quartz veins of 1 mm–15 cm thickness, yielding rather high quartz content (in average 40%), together with feldspars, garnets and amphiboles. The quaternary geology of the island has previously been mapped (Andreassen et al., 1985), reporting traces of past shore lines and deposits from active cirque glaciers and permafrost. Most of the cirques at Arnøy contain multiple moraines, but do not hold glaciers at present. In fact, only two glaciers are still present on the island and they are located along the eastern mountain ridge. These two glaciers are the target in this study. Rødhetta (1.1 km^2) and Nymoen (0.8 km^2) glaciers are small mountain glaciers. Rødhetta glacier has a relatively simple configuration with only one major accumulation area and a simple valley geometry. The Rødhetta glacier moraine chronology, complemented by moraines from the neighboring glacier Nymoen and the Snøfonn snow-field are presented in Fig. 1. These glaciers display well resolved and -preserved moraine sequences topped by large embedded boulders that are the target of our ^{10}Be surface exposure dating study (see also Fig. 3).

2.2. Geomorphic setting

We identified and mapped 13 moraine ridges (M1-M13, Fig. 1) deposited by the Rødhetta Glacier. For the Nymoen Glacier and the Snøfonn forefield, we focus on the outermost LG moraine, but mapped also the entire moraine sequences (Fig. 1).

2.2.1. Rødhetta moraines

Our detailed geomorphic map (Fig. 1) groups the Rødhetta moraine sequence into three sub-sequences, presented from old to young:

(i) The outermost moraine sequence (M1-M4; 120 - 65 m a.s.l.) consists of four individual ridges (red moraines in Fig. 1). The ~80 m high moraine sequence (LG, Fig. 1) includes four partly continuous, elongated ridges deposited ~200 m away from the present-day shoreline. The distal slope of the moraine complex displays a number of abrasion terraces. The four individual terminal moraines (M1-M4) are ~500–800 m long, overall arcuate and on a smaller scale winding in shape, reflecting the glacier terminus during moraine formation (Benn and Evans, 2014). The moraine sides have similar ice-distal and ice-proximal angles (~35–40°); the moraine crests are rounded. Several meltwater channels cut through the terminal moraines. We interpret M1-M4 to be push moraines representing oscillatory glacier advances and explain the symmetric shape by post-depositional erosion.

(ii) Inboard of the outermost moraine sequence, there is a steep slope (angle >20°) upwards to the intermediate moraine sequence (330-160 m a.s.l.), which consists of six partly continuous, arcuate elongated ridges (M5-M10) (light purple moraines in Fig. 1). The ridges are ~70–1200 m long and ~5–50 m high, and display ice-distal and ice-proximal angles which are similar on individual ridges (~20–40°); the moraine crests are rounded. The moraine loops and ridge

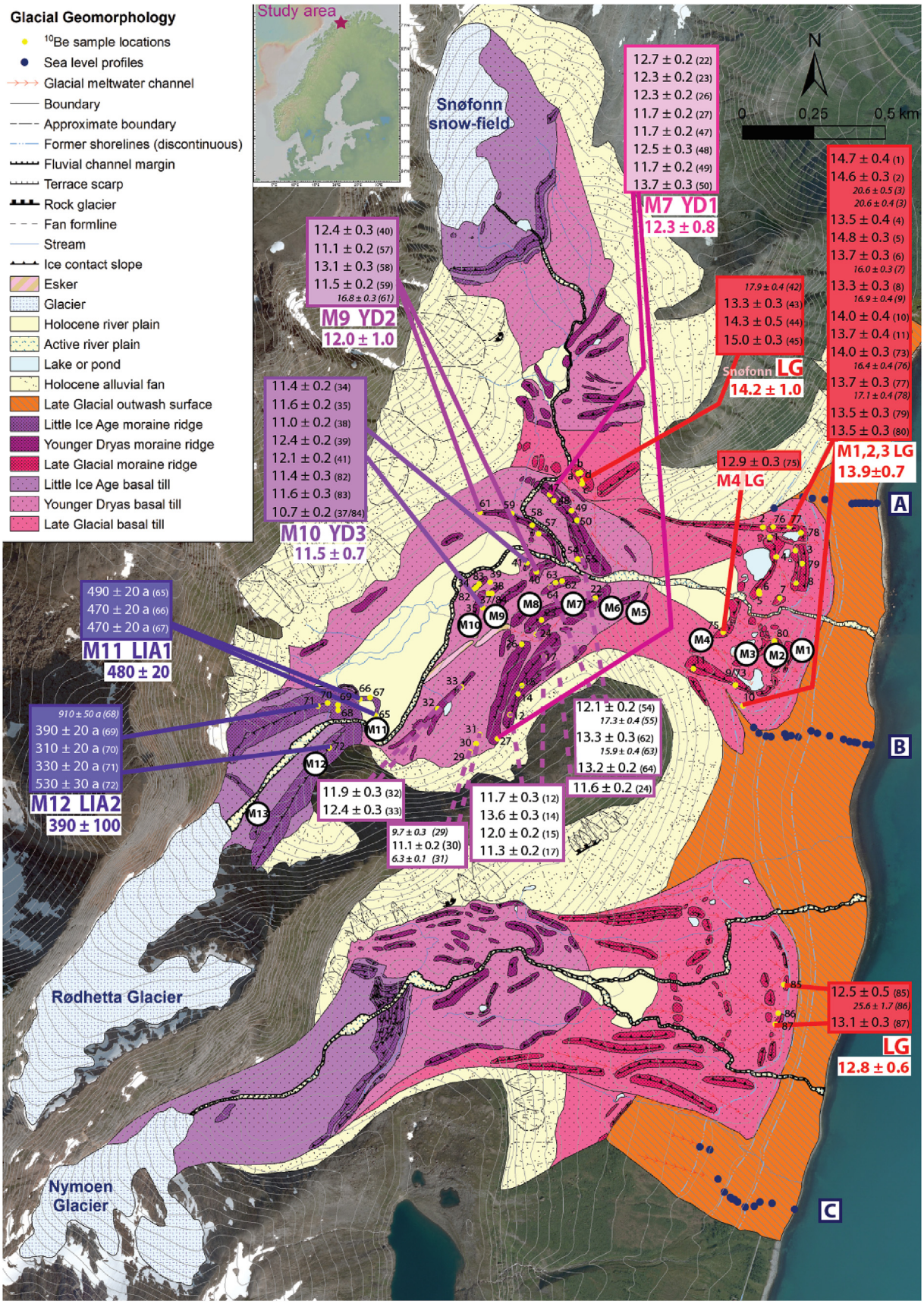

Fig. 1. Geomorphic map of the Late Glacial and Holocene moraine sequences of Rødhetta Glacier (M1 to M13), Nymoen Glacier and Snøfonn snow-field, along with the ^{10}Be moraine chronology. Colored dots indicate the ^{10}Be boulder sample locations. In the color-coded boxes, we provide the ^{10}Be boulder ages in ka (LIA ages are given in a) within 1σ analytical uncertainties and sample numbers/letters. Below each respective box, we show the arithmetic means of the boulder ages, which we interpret as their moraine ages/glacier

fragments reflect the margins of the former glaciers. We interpret M5-M10 as push moraines representing oscillatory glacier advances punctuating the general retreat of Rødhetta Glacier. M7 (YD1, Fig. 1) is a prominent ridge observed across the whole valley. Proximal of M8, a ~350 m long esker is connected to a former meltwater channel that cuts through M8 and M7. M9 (YD2, Fig. 1) is a well-preserved moraine loop. M10 (YD3, Fig. 1) consists of relatively flat and partly undulating ridge fragments, assigned to a composite moraine genesis of repeatedly pushing ice margins.

(iii) The innermost Rødhetta moraine sequence consists of three distinct moraine ridges (M11-M13; 390-210 m a.s.l.; dark purple moraines in Fig. 1) and is located ~800 m from the intermediate sequence at the bottom of a steep slope towards today's glacier. The ridges are ~110–1100 m long and have a 'fresh' geomorphic appearance: they feature distinct crests and lack vegetation cover. The cross-sectional profiles display steeper distal than proximal latero-frontal angles (~40° vs. 35°), implying push moraine genesis. This geomorphologic feature is more pronounced on these younger, well-preserved moraines, than on the older, more eroded moraines of the intermediate and outermost sequences. M11 (LIA1, Fig. 1) is a 1 m high ridge that overtops a glacio-fluvial delta (2–4° inclination) on the ice-proximal side. M12 (LIA2, Fig. 1) is a well-preserved moraine loop up to 35 m high. We interpret M11-M13 to be push moraines representing oscillatory advances of Rødhetta Glacier.

2.2.2. Nymoen moraines

The Nymoen Glacier and its moraine sequence show high consistency to the Rødhetta system; therefore we do not add an individual description for Nymoen here.

2.2.3. Snøfonn moraines

Snøfonn is a perennial snow-field, so changes in amplitude do not exclusively reflect changes in climate and are therefore unsuitable for ELA quantifications and climate implications. In addition, the mapping of the Snøfonn snow-field moraine sequence is not unambiguous. The outermost terminal moraine (320-290 m a.s.l.) is ~300 m long and up to 40 m high. The ice-distal angle of the moraine flank is 30°; the ice-proximal moraine shape is of undulating, composite character.

2.2.4. Shorelines

Geomorphic shoreline mapping shows that the Rødhetta and Nymoen Glaciers were land-based when depositing the moraines. The Marine Limit, representing the sea level high-stand of the region, is observed at 64 m a.s.l. in the study area (profiles A, C, Figs. 1 and S1 and S2). This sea level high-stand has earlier been correlated to the Risvik sub-stage in Finnmark, more than 15 ka ago (Bakke et al., 2005; Sollid et al., 1973).

A meltwater channel located distal of the northern lateral branch of the outermost LG moraine sequence of Rødhetta Glacier terminates in a delta at the Marine Limit (profile A in Fig. 1). The delta is ~40 m long and equally broad at the outer opening. Delta formation must have occurred coevally to the deposition of the outermost LG moraine ridge, because only then was the extent of Rødhetta Glacier sufficiently large to drain meltwater into this channel. The presence of the delta implies that the meltwater channel terminated into the sea and implies that Rødhetta Glacier was not subject to complex calving processes during its full LG configuration. The Main shoreline (YD) at 41 m a.s.l., and the Tapes shoreline (Holocene transgression) at 16 m a.s.l. (Figs. S1 and S2) were observed as prominent beach ridges and abrasion terraces (Fig. 1).

3. Methods

The samples were processed at the Cosmogenic Nuclide Laboratory at the Lamont-Doherty Earth Observatory (LDEO) following the standard geochemical approach for quartz preparation and beryllium extraction (Schaefer et al., 2009).

All samples were measured at the Center of Accelerator Mass Spectrometry at the Lawrence Livermore National Laboratory; all $^{10}Be/^{9}Be$ ratios were normalized to the 07KNSTD standard (Nishiizumi et al., 2007).

3.1. Production rate and ^{10}Be ages

To calculate individual ^{10}Be boulder ages from the ^{10}Be concentrations (Table 1) we used the most recent 'Version 3' of the cosmogenic 'Online Calculators (https://hess.ess.washington.edu/math/v3/v3_age_in.html), together with the local Arctic Production Rate of 3.96 ± 0.15 atoms g^{-1} a^{-1}, which was established based on high-quality data sets in Arctic Canada and Greenland (Young et al., 2013) and the 'St' scaling for altitude and latitude, which agrees with the 'Lm' and 'LSD' scalings (Tables 1 and 2). We also show for completeness the ages based on the default 'global production rate' embedded in the Version 3 Calculators, which gives ages about 1.5% younger than the local Arctic Production rate within the 'St' and 'Lm' scaling schemes, but >9% younger if the 'LSD' scaling is applied. The LG Arctic Production Rate agrees with the North American Production Rate presented by (Balco et al., 2009), and is consistent with recently published production rate calibration experiments in Norway (Fenton et al., 2011), Scotland (Putnam et al., 2019), the Swiss Alps (Claude et al., 2014), as well as with recent production rate calibrations from the southern hemisphere, such as New Zealand (Putnam et al., 2010a) and Patagonia (Kaplan et al., 2011). These converging production rates suggest that paleo climate related air pressure changes potentially modulating the production rates (Staiger et al., 2007) are either rather homogenous or play a minor role in this context. None of the climate conclusions below depend on the choice of production rate or the scaling scheme. We list the boulder ages with 1 σ analytical uncertainties in Table 2.

Snow cover and erosion of boulder surfaces: Snow cover of the sampled surfaces over a considerable period of time would reduce the cosmogenic nuclide production rate and thus would lead to an underestimation of the true exposure age. To minimize this potential problem we took the following steps: (i) We sampled only large boulders, most of them on moraine crests and thus exposed to strong winds, minimizing the likelihood that snow can accumulate on top of those boulders longer periods; (ii) The relative large number of sampled boulders and the internal consistency of the exposure ages argue against significant snow-cover, as this effect

culmination ages. The moraine age error includes the standard error of the arithmetic mean and the local production rate uncertainty given by (Young et al., 2013). Red boxes indicate the Rødhetta Late Glacial culmination moraine (M1-M3) and the Snøfonn snow-field and Nymoen Glacier equivalents. Pink boxes represent the three-stepwise retreat of Rødhetta Glacier through the Younger Dryas stadial (M7, M9-M10). Purple boxes show the historical glacier advances during the Little Ice Age (M11-M12). The ages in the white boxes are from boulders in less well constrained or ambiguous stratigraphic positions and/or not on one of our focus moraines. The ages of these boulders, while generally consistent with the boulder ages from well-defined positions, show overall higher scatter, and are not further discussed due to the geomorphic-stratigraphic ambiguity. Outliers are marked with small italic font. (For interpretation of the references to color in this figure legend, the reader is referred to the Web version of this article.)

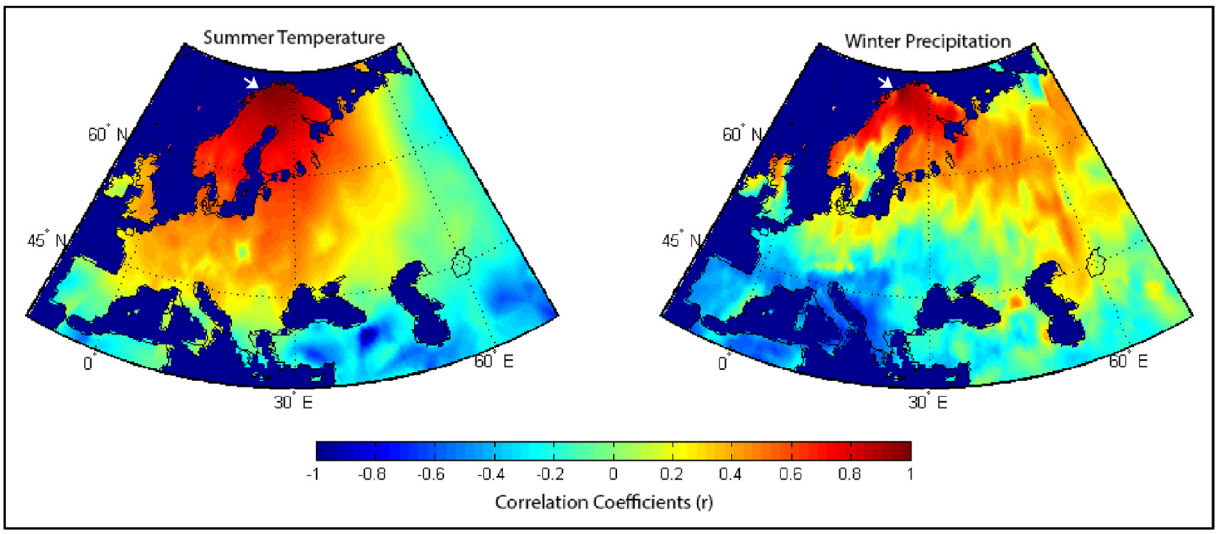

Fig. 2. Correlations of mean summer temperature (May to September) and total winter precipitation (October to April) at Rødhetta Glacier with each 10′ grid locations across Europe and bordering regions. Data are from the CRU 1.2 and CRU 3.21 monthly gridded data from 1901 to 2000 CE (Harris et al., 2013; Mitchell et al., 2004). White arrows indicate the location of the Island of Arnøya. These maps illustrate the high spatial correlation of climate variability at Arnøya with surrounding regions. The spatial correlation is even higher for summer temperature than for winter precipitation.

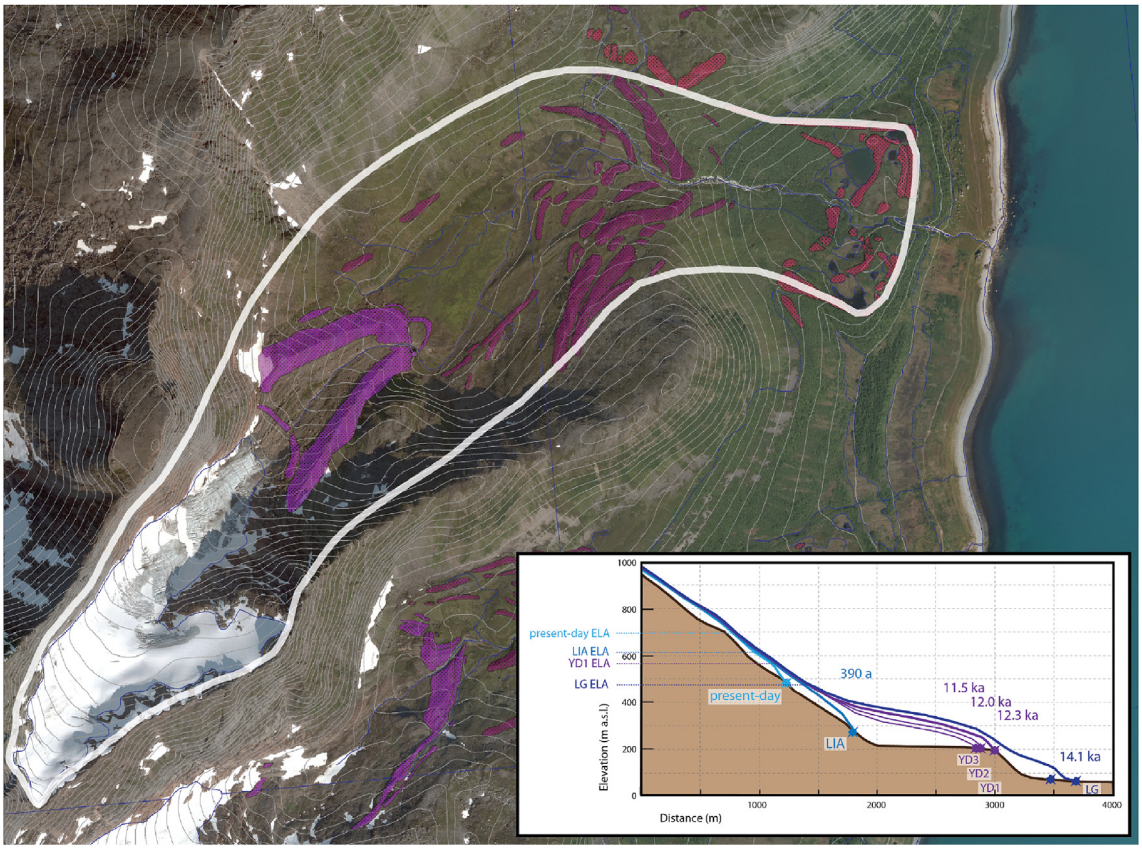

Fig. 3. The main panel shows the reconstructed Rødhetta Glacier during its Late Glacial culmination 13.9 ± 0.7 ka ago. The inset shows the color-coded flow-line modeled cross-sections for Rødhetta Glacier in present-day (2013 CE), historic (LIA), Younger Dryas (YD) and Late Glacial (LG) extents, with respective equilibrium line altitudes (dotted lines). Locations of moraines are marked with stars. See also Fig. S3. (For interpretation of the references to color in this figure legend, the reader is referred to the Web version of this article.)

should produce larger scatter in exposure ages; (iii) We list in Table 1 the different boulders according to their shape, because pyramide-shaped boulders should be less affected by snow-cover than altar-shaped boulders. We do not detect any relation of exposure ages and boulder shape.

Boulders have been shown to be resistant to erosion on time-

Table 1
Geographical and analytical data for all 71 samples. Outliers in the moraine chronology are italicized. The exceptional high shielding factor of sample ROD-12-9 results from sampling on the boulder side.

Sample	Latitude	Longitude	Altitude (m)	air pressure	Thickness (cm)	Density (g cm-3)	Shielding	Erosion	Year sampled;	Nuclide	Mineral	10Be (at g-1)	1 Sigma	AMS Standard;
Rødhetta LG Outermost moraine sequence (Ml, M2, M3)														
ROD-12-1	70.166	20.779	80	std	1.79	2.7	0.98	0	2012	Be-10	quartz	6.67E+04	1.80E+03	07KNSTD;
ROD-12-2	70.167	20.778	76	std	1.91	2.7	0.96	0	2012;	Be-10	quartz	6.46E+04	1.48E+03	07KNSTD;
ROD 12-3a	*70.166*	*20.781*	*71*	*std*	*2.32*	*2.7*	*0.98*	*0*	*2012;*	*Be-10*	*quartz*	*9.17E+04*	*2.10E+03*	*07KNSTD;*
ROD-12-3b	*70.165*	*20.777*	*71*	*std*	*2.32*	*2.7*	*0.98*	*0*	*2012;*	*Be-10*	*quartz*	*9.20E+04*	*1.84E+03*	*07KNSTD:*
ROD-12-4	70.166	20.779	74	std	1.83	2.7	0 98	0	2012;	Be-10	quartz	6.05E+04	1.77E+03	07KNSTD;
ROD-12-5	70.165	20.777	73	std	2.66	2.7	099	0	2012;	Be-10	quartz	6.65E+04	1.53E+03	07KNSTD;
ROD-12-6	70.165	20.777	72	std	2.39	2.7	0.99	0	2012;	Be-10	quartz	6.18E+04	1.49E+03	07KNSTD;
ROD-12 7	*70.164*	*20.779*	*68*	*std*	*2.81*	*2.7*	*0.99*	*0*	*2012;*	*Be-10*	*quartz*	*7.16E+04*	*1.54E+03*	*07KNSTD;*
ROD-12-8	70.165	20.781	67	std	1.97	2.7	0.99	0	2012;	Be-10	quartz	6.00E+04	1.42E+03	07KNSTD;
ROD 12-9	*70.162*	20.774	*80*	*std*	*3.59*	*2.7*	0.78	*0*	*2012;*	*Be-10*	*quartz*	*6.03E+04*	*1.50E+03*	*07KNSTD;*
ROD-12-10	70.161	20.775	67	std	2.5	2.7	0.98	0	2012;	Be-10	quartz	6.24E+04	1.66E+03	07KNSTD;
ROD-12-11	70.163	20.770	118	std	1.87	2.7	0.98	0	2012;	Be-10	quartz	6.45E+04	1.65E+03	07KNSTD;
ROD-13-73	70.162	20.774	80	std	1.25	2.7	0.99	0	2013;	Be-10	quartz	6.41E+04	1.22E+03	07KNSTD;
ROD 13-76	*70.167*	*20.779*	*70*	*std*	*0.8*	*2.7*	0.97	*0*	*2013;*	*Be-10*	*quartz*	*7.32E+04*	*1.67E+03*	*07KMSTD;*
ROD-13-77	70.167	20.781	64	std	1.62	2.7	0.97	*0*	2013;	Be-10	quartz	6.07E+04	1 39E+03	07KNSTD;
ROD 13 78	*70.166*	*20.782*	*62*	*std*	*0.99*	*2.7*	*0.98*	*0*	2013;	*Be 10*	*quartz*	*7.65E+04*	*1.75E+03*	*07KNSTD;*
ROD-13-79	70.165	20.781	66	std	*2.2*	2.7	0.98	*0*	2013;	Be-10	quartz	6.01E+04	1.50E+03	07KNSTD;
ROD-13-80	70.163	20.778	81	std	1.25	2.7	0.96	0	2013;	Be-10	quartz	6.04E+04	1.47E+03	07KNSTD;
Rødhetta LG inner moraine (M4)														
ROD-13-75	70.164	20.774	71	std	4.09	2.7	097	0	2013;	Be-10	quartz	5.64E+04	1.14E+03	07KNSTD;
Rødhetta Intermediate - YD1 (M7)														
ROD-12-22	70.165	20.762	222	std	2.56	2.7	0.99	0	2012,	Be-10	quartz	6.67E+04	1.30E+03	07KNSTD;
ROD-12-23	70.164	20.757	256	std	2.51	2.7	0.99	0	2012;	Be-10	quartz	6.70E+04	1.31E+03	07KNSTD;
ROD-12-26	70.164	20.755	272	std	2.84	2.7	0.99	0	2012;	Be-10	quartz	6.80E+04	1.33E+03	07KNSTD;
ROD-12-27	70.161	20.752	314	std	3.73	2.7	0.98	0	2012;	Be-10	quartz	6.63E+04	1.29E+03	07KNSTD;
ROD-12-47	70.168	20.759	271	std	2.99	2.7	0.98	0	2012;	Be-10	quartz	6.39E+04	1.33E+03	07KNSTD;
ROD-12-48	70.168	20.759	269	std	2.69	2.7	098	0	2012;	Be-10	quartz	6.83E+04	1 37E+03	07KNSTD;
ROD-12-49	70.168	20.761	249	std	1.04	2.7	098	0	2012;	Be-10	quartz	6.31E+04	1.17E+03	07KNSTD;
ROD-12-50	70.168	20.761	244	std	2.48	2.7	0.99	0	2012;	Be-10	quartz	7.35E+04	1 66E+03	07KNSTD;
Rødhetta Intermediate - YD2 (M9)														
ROD-12-40	70.166	20.757	219	std	2.31	2.7	0.98	0	2012;	Be-10	quartz	6.47E+04	1.40E+03	07KNSTD;
ROD-12-57	70.167	20.757	217	std	2.26	2.7	0.98	0	2012;	Be-10	quartz	5.76E+04	1.15E+03	07KNSTD;
ROD-12-58	70.167	20.757	226	std	1.78	2.7	0.96	0	2012;	Be-10	quartz	6.77E+04	1.59E+03	07KNSTD;
ROD-12-59	70.168	20.755	227	std	1.49	2.7	0 97	0	2012;	Be-10	quartz	6.01E+04	1 14E+03	07KNSTD;
ROD-12 61	*70.168*	*20.752*	*239*	*std*	*2.33*	*2.7*	*0.96*	*0*	*2012;*	*Be-10*	*quartz*	*S. 71E+04*	*1.65E+03*	*07KNSTD;*
Rødhetta Intermediate - YD3 (M10)														
ROD-12-34	70.166	20.751	222	std	3.11	2.7	0 97	0	2012;	Be-10	quartz	5.86E+04	1 12E+03	07KNSTD;
ROD-12-35	70.165	20.752	230	std	2.79	2.7	097	0	2012;	Be-10	quartz	6.04E+04	1 22E+03	07KNSTD;
ROD-12-38	70.165	20.753	221	std	2.78	2.7	098	0	2012;	Be-10	quartz	5.70E+04	1 08E+03	07KNSTD;
ROD-12-39	70.166	20.752	219	std	2.61	2.7	097	0	2012;	Be-10	quartz	6.36E+04	1 18E+03	07KNSTD;
ROD-12-41	70.166	20.756	217	std	2.45	2.7	097	0	2012;	Be-10	quartz	6.19E+04	1 16E+03	07KNSTD;
ROD-13-82	70.166	20.751	222	std	1.47	2.7	097	0	2013;	Be-10	quartz	5.94E+04	1 43E+03	07KNSTD;
ROD-13-83	70.166	20.751	222	std	1.45	2.7	0.97	0	2013;	Be-10	quartz	6.02E+04	1.49E+03	07KNSTD;
ROD-12-37	70.166	20.752	221	std	2.07	2.7	0.97	0	2012;	Be-10	quartz	5.58E+04	1 06E+03	07KNSTD;
ROD-13-84 (duplicate −37)	70.166	20.752	221	std	2.09	2.7	0.97	0	2013;	Be-10	quartz	5.48E+04	1 36E+03	07KNSTD;
Rødhetta Innermost - LIA1 (Mil)														
ROD-12-65	70.162	20.741	217	std	2.36	2.7	0.93	0	2012;	Be-10	quartz	2.43E+03	1.21E+02	07KNSTD;
ROD-12-66	70.163	20.739	217	std	1.45	2.7	0.93	0	2012;	Be-10	quartz	2.33E+03	1.17E+02	07KNSTD;
ROD-12-67	70.163	20.740	217	std	2.57	2.7	0.93	0	2012;	Be-10	quartz	2.30E+03	1.15E+02	07KNSTD;
Rødhetta Innermost - LIA2 (M12)														
ROD-12-68	*70.162*	20.737	254	*std*	*1.88*	*2.7*	*0.93*	0	*2012;*	*Be-10*	*quartz*	*4.69E+03*	*2.34E+02*	*07KNSTD;*
ROD-12-69	70.162	20.737	248	std	2.71	2 7	0.94	0	2012	Be-10	quartz	2.02E+03	1.01E+02	07KNSTD;
ROD-12-70	70.162	20.736	250	std	2.86	2.7	0.93	0	2012;	Be-10	quartz	1.58E+03	7.91E+01	07KNSTD;
ROD-12-71	70.162	20.736	261	std	3.9	2.7	0.92	0	2012;	Be-10	quartz	1.67E+03	8.35E+01	07KNSTD;
ROD-12-72	70.161	20.736	282	std	1.46	2.7	0.92	0	2012;	Be-10	quartz	2.80 E+03	1.40E+02	07KNSTD;
Nymoen LG														
NYM-13-85	70.152	20.776	75	std	1.21	2.7	1	0	2013;	Be-10	quartz	5.77E+04	2.17E+03	07KNSTD;
NYM-13-86	*70.152*	*20.775*	*69*	*std*	*0.88*	*2.7*	*1*	*0*	*2013;*	*Be-10*	*quartz*	*1.176+05*	*7.65 6+03*	*07KNSTD;*
NYM-13-87	70.151	20.775	70	std	1.57	2.7	1	0	2013;	Be-10	quartz	5.99E+04	1.17E+03	07KNSTD;
Snøfonn LG Outermost														
ROD-12-42	70.169	20.762	296	std	2.89	2.7	0.99	0	2012;	Be-10	quartz	1.01E+05	2.16E+03	07KNSTD;
ROD-12-43	70.169	20.762	296	std	2.59	2.7	0.99	0	2012;	Be-10	quartz	7.51E+04	1.94E+03	07KNSTD;
ROD-12-44	70.169	20.762	292	std	3.13	2.7	0.99	0	2012;	Be-10	quartz	7.99E+04	2.65E+03	07KNSTD;
ROD-12-45	70.169	20.762	294	std	2.34	2.7	0.99	0	2012;	Be-10	quartz	8.46E+04	1.69E+03	07KNSTD;
Additional Samples Rødhetta														
ROD-12-12	70.162	20.753	318	std	2.3	2.7	0.99	0	2012	Be-10	quartz	6.75E+04	1.50E+03	07KNSTD;
ROD-12-14	70.162	20.754	307	std	3.55	2 7	0.99	0	2012;	Be-10	quartz	7.72E+04	1.44E+03	07KNSTD;
ROD-12-15	70.163	20.755	303	std	2.37	2.7	0.99	0	2012;	Be-10	quartz	6.85E+04	1.28E+03	07KNSTD;
ROD-12-17	70.163	20.757	287	std	2.97	2 7	0.99	0	2012;	Be-10	quartz	6.31E+04	1.18E+03	07KNSTD;

Table 1 (*continued*)

Sample	Latitude	Longitude	Altitude (m)	air pressure	Thickness (cm)	Density (g cm-3)	Shielding	Erosion	Year sampled;	Nuclide	Mineral	10Be (at g-1)	1 Sigma	AMS Standard;
ROD-12-24	70.164	20.756	266	std	3.29	2.7	0.98	0	2012;	Be-10	quartz	6.25E+04	1.22E+03	07KNSTD;
ROD-12-29	*70.161*	*20.749*	*297*	*std*	*2.72*	2.7	*0.96*	*0*	*2012*	*Be-10*	*quartz*	*5.30E+04*	*1.386+03*	*07KNSTD;*
ROD-12-30	*70.161*	*20.750*	*299*	*std*	*2.27*	*2.7*	*0.97*	*0*	*2012;*	*Be-10*	*quartz*	*6.176*04*	*1.326+03*	*07KN5TD;*
ROD-12-31	*70.161*	*20.750*	*294*	*std*	*2.06*	*2.7*	*0.97*	*0*	*2012;*	*Be-10*	*quartz*	*3.526+04*	*7.54E+02*	*07KNSTD;*
ROD-12-32	70.162	20.747	239	std	2.1	2.7	0.96	0	2012;	Be-10	quartz	6.24E+04	1.64E+03	07KNSTD;
ROD-12-33	70.168	20.759	244	std	2.73	2.7	0.97	0	2012;	Be-10	quartz	6.53E+04	1.47E+03	07KNSTD;
ROD-12-54	70.166	20.761	205	std	2.07	2.7	0.96	0	2012;	Be-10	quartz	6.11E+04	1.20E+03	07KNSTD;
ROD-12-55	*70.166*	*20.761*	*204*	*std*	*2.25*	*2.7*	*0.98*	*0*	*2012;*	*Be-10*	*quartz*	*8.846+04*	*1.816+03*	*07KNSTD;*
ROD-12-62	70.166	20.759	209	std	2.29	2.7	0.98	0	2012;	Be-10	quartz	6.87E+04	1.30E+03	07KNSTD;
ROD-12-63	*70.166*	*20.759*	*213*	*std*	*1.6*	*2.7*	*0.98*	0	*2012;*	*Be-10*	*quartz*	*8.266+04*	*1.876+03*	*07KNSTD;*
ROD-12-64	70.165	20.758	215	std	1.87	2.7	0.98	0	2012;	Be-10	quartz	6.84E+04	1.29E+03	07KNSTD;

scales much longer than the interval considered here, we therefore neglect surface erosion in our age calculations. Note that an erosion rate of 1 mm/ka, frequently used in the literature to somehow account for erosion, would increase the ages systematically by 1.2%, not impacting any of the conclusions made below.

Moraine Ages: To derive a moraine age, wwe calculate the arithmetic mean of the ^{10}Be boulder ages from one moraine (2 σ outliers excluded, see Fig. 4). We interpret these moraine ages as the termination of the respective glacier advance, as these boulders were deposited at the very end of the respective moraine formation period, just before the onset of glacier retreat. The uncertainty of these ^{10}Be moraine ages include (i) the standard deviation of arithmetic mean of the ^{10}Be boulder ages from the respective moraine, (ii) the production rate uncertainty given above, and (iii) a 1% uncertainty for the ^{9}Be carrier concentration produced and calibrated at LDEO.

3.2. Glacier modeling and climatic implications

We present and applied a flexible, first-order ELA model based on geomorphic constraints to estimate changes in ELA underlying the reconstructed glacier advances, and then derive a range of temperature and precipitation changes required to drive the ELA changes. All details of this model approach are given in (Supplementary Material).

Reconstructing ELAs: The ELA is the altitude on a glacier where total annual snow accumulation, or mass gain, equals the total annual ablation, or mass loss (Cuffey and Paterson, 2010). Directly related to climate, the ELA provides a common measure that can be compared from one region to another and represents one of the most useful glaciological measures for climate reconstructions (Cuffey and Paterson, 2010; Lüthi, 2014; Porter, 1975).

Briefly, the ELA model captures the relationship between the ELA and glacier hypsometry, and accounts for changes in bed slope, glacier thickness, and relative valley widths. This is important for Rødhetta Glacier, as the slope of the bed changes significantly down-valley. In addition, glacier thickness in the model is a function of both glacier length and slope (Oerlemans, 2001), thus accounting for feedbacks that naturally occur as a glacier changes size.

Climate Drivers of the ELA changes: We use the observed mass balance gradients in Norway to calculate the mass balance changes associated with the modeled changes in ELAs (e.g., Rupper and Roe, 2008; Rasmussen and Andreassen, 2005; Cuffey and Paterson, 2010). This is directly analogous to using temperature lapse rates to calculate the change in temperature for a given change in elevation, but avoids the assumption that temperature is the only parameter influencing mass balance or ELA changes. We then estimate climate change from the mass balance changes for two endmember scenarios: changes in precipitation only and changes in temperature only. For the scenario where we assume only change in precipitation (and no change in temperature), changes in snow accumulation are directly equal to the mass balance changes and requires no further modeling or calculations. For the scenario where we assume only change in temperature (and no change in precipitation), the mass balance changes are driven entirely by changes in ablation. We model the change in temperature for the estimated change in ablation using the commonly applied positive degree day approach (e.g., Braithwaite and Zhang (2000); Cuffey and Paterson (2010); Hock (2003)). This approach has been shown to be useful in mountain glacier settings with a significant correlation between temperature and ablation (for example, in the Alps; Six and Vincent (2014); Thibert et al. (2013); Vincent and Vallon (1997)). We account for the uncertainties in the reconstructed ELAs, mass balance gradient, and positive degree day ablation model using a Monte Carlo approach, thereby providing the range in temperature and precipitation reconstructions that can reasonably explain the reconstructed glacier changes. All details of this approach are provided in the Supplementary Material (see also Fig. 3).

4. Results

The geomorphic map (Fig. 1) shows the 13 moraine ridges mapped in front of Rødhetta Glacier (M1-M13), its tributary snowfield Snøfonn and the neighboring Nymoen Glacier.

Our moraine chronology consists of 71 ^{10}Be boulder ages (Table 2, Figs. 1 and 4), ranging from ~14 ka ago to the Little Ice Age (LIA) (1300–1850 CE), with 1σ analytical uncertainties of 2–3% for the LG moraine boulder ages and 5–7% for the historic moraine boulder ages. 64 dates come from the Rødhetta moraine sequence, 49 of those are from the most prominent and best-preserved moraines that are the core of the Rødhetta glacier chronology. Samples with less well-defined stratigraphic positions are shown in Fig. 1 in white boxes. Eight boulders are from the Rødhetta LIA moraines; four samples were dated from the Snøfonn LG moraines, and three from the Nymoen LG moraines (Tables 1 and 2).

Individual boulder ages from the outermost Rødhetta LG moraine sequence (M1-M3, Fig. 1) range from 13.3 ± 0.3 ka to 14.8 ± 0.3 ka (n = 18 ^{10}Be ages, excluding five 2σ outliers, with one duplicate measurement of sample 3), with a mean of 13.9 ± 0.7 ka, dating the LG culmination of Rødhetta Glacier prior to the YD stadial. A single boulder age from the inner ridge M4 (sample 75) yields an age of 12.9 ± 0.5 ka, consistent with the stratigraphic order of these moraines. This age is corroborated by the LG boulder ages of Nymoen Glacier, dating to 12.8 ± 0.6 ka (n = 3, excluding one 2σ outlier). The boulder ages from the outermost moraine of Snøfonn snow-field date to 14.2 ± 1.0 ka (n = 4, excluding one 2σ outlier).

The ^{10}Be ages from the three dated moraines (M7, M9, M10) of

Table 2
^{10}Be ages of all 71 samples with 1σ analytical errors (see Methods for error discussion), based on the Arctic Production Rate (Young et al., 2013) and based on three commonly used scaling protocols. Ages based on 'Lm' scaling, which is the time dependent version of the 'St' scaling presented by (Lal, 1991) and updated by (Stone, 2000), are identical. Ages based on the 'LSD' scaling are 1% higher. Last column: 'a' = altar-shaped, 'p' = pyramid-shaped boulders; outliers are not related to boulder-shape and thus snow-cover does not impact this chronology. Ages are calculated assuming no erosion, as we do not have evidence for erosion of these surfaces. An erosion rate of 1 mm/ka, which is hypothesized in some papers, would increase all ages by 1.2%, without any impact on the conclusions of this paper.

Sample name	Nuclide	St		Lm		LSDn		
		Age (yr)	error (yr)	Age (yr)	error (yr)	Age (yr)	error (yr)	
Rødhetta LG Outermost moraine sequence (MI, M2, M3)								
ROD-12-1	Be-10 (qtz)	14,717	399	14,716	399	14,719	399	P
ROD-12-2	Be-10 (qtz)	14,622	336	14,622	336	14,618	336	a
ROD-12-4	Be-10 (qtz)	13,445	394	13,445	394	13,423	394	P
ROD-12-5	Be-10 (qtz)	14,745	340	14,745	340	14,733	340	P
ROD-12-6	Be-10 (qtz)	13,681	331	13,681	331	13,667	331	P
ROD-12-8	Be-10 (qtz)	13,307	316	13,307	316	13,284	315	P
ROD-12-lO	Be-10 (qtz)	14,042	375	14,042	375	14,021	374	P
ROD-12-11	Be-10 (qtz)	13,672	351	13,671	351	13,723	352	P
ROD-13-73	Be-10 (qtz)	13,948	266	13,937	266	13,937	266	P
ROD-13-77	Be-10 (qtz)	13,742	316	13,742	316	13,715	315	P
ROD-13-79	Be-10 (qtz)	13,504	338	13,504	338	13,480	338	P
ROD-13-80	Be-10 (qtz)	13,520	330	13,520	330	13,520	330	a
ROD-12-3a	*Be-10 (qtz)*	*20,549*	*473*	*20,549*	*473*	*20,556*	*473*	*P*
ROD-12-3b	*Be-10 (qtz)*	*20,617*	*414*	*20,616*	*414*	*20,624*	*415*	*P*
ROD-12-7	*Be-10 (qtz)*	*15,984*	*345*	*15,983*	*345*	*15,970*	*345*	*P*
ROD-12-9	*Be-10 (qtz)*	*16,900*	*422*	*16,900*	*422*	*16,912*	*422*	*P*
ROD-13-76	*Be-10 (qtz)*	*16,364*	*375*	*16,363*	*375*	*16,355*	*375*	*P*
ROD-13-78	*Be-10 (qtz)*	*17,107*	*393*	*17,107*	*393*	*17,085*	*393*	*P*
Rødhetta LG inner moraine (M4)								
ROD-13-75	Be-10 (qtz)	12,929	262	12,929	262	12,911	262	a
Rødhetta Intermediate - YD1 (M7)								
ROD-12-22	Be-10 (qtz)	12,649	247	12,639	247	12,782	250	a
ROD-12-23	Be-10 (qtz)	12,262	240	12,262	240	12,423	244	P
ROD-12-26	Be-10 (qtz)	12,281	241	12,281	241	12,452	244	a
ROD-12-27	Be-10 (qtz)	11,686	228	11,686	228	11,867	232	a
ROD-12-47	Be-10 (qtz)	11,681	244	11,681	244	11,840	247	a
ROD-12-48	Be-10 (qtz)	12,482	251	12,482	251	12,655	255	a
ROD-12-49	Be-10 (qtz)	11,653	216	11,603	216	11,747	218	a
ROD-12-50	Be-10 (qtz)	13,646	309	13,616	309	13,793	313	P
Rødhetta Intermediate - YD2 (M9)								
ROD-12-40	Be-10 (qtz)	12,394	269	12,394	269	12,532	272	P
ROD-12-57	Be-10 (qtz)	11,048	221	11,048	221	11,151	223	a
ROD-12-58	Be-10 (qtz)	13,086	308	13,086	308	13,240	312	a
ROD-12-59	Be-10 (qtz)	11,455	218	11,455	218	11,583	220	a
ROD-12-61	*Be-10 (qtz)*	*16,747*	*318*	*16,707*	*318*	*16,934*	*322*	P
Rødhetta Intermediate - YD3 (M10)								
ROD-12-34	Be-10 (qtz)	11,377	218	11,377	218	11,500	220	a
ROD-12-35	Be-10 (qtz)	11,602	235	11,602	235	11,734	238	a
ROD-12-38	Be-10 (qtz)	10,935	208	10,935	208	11,047	210	a
ROD-12-39	Be-10 (qtz)	12,347	230	12,337	230	12,474	232	a
ROD-12-41	Be-10 (qtz)	12,055	226	12,015	226	12,145	228	P
ROD-13-82	Be-10 (qtz)	11,377	275	11,377	275	11,500	278	P
ROD-13-83	Be-10 (qtz)	11,549	286	11,529	286	11,655	289	P
ROD-12-37	Be-10 (qtz)	10,750	205	10,750	205	10,856	207	P
ROD-13-84 (duplicate to −37)	Be-10 (qtz)	10,659	263	10,559	263	10,651	265	P
Rødhetta Innermost - LIA1 (M11)								
ROD-12-65	Be-10 (qtz)	490	24	490	24	481	24	a
ROD-12-66	Be-10 (qtz)	466	23	466	23	460	23	P
ROD-12-67	Be-10 (qtz)	465	23	464	23	458	23	a
Rødhetta Innermost - LIA2 (M12)								
ROD-12-68	*Be-10 (qtz)*	*907*	*45*	*907*	*45*	*878*	*44*	P
ROD-12-69	Be-10 (qtz)	392	20	392	20	392	20	a
ROD-12-70	Be-10 (qtz)	309	15	309	15	312	16	P
ROD-12-71	Be-10 (qtz)	330	16	330	16	332	17	P
ROD-12-72	Be-10 (qtz)	531	27	531	27	520	26	P
Nymoen LG								
NYM-13-85	Be-10 (qtz)	12,481	471	12,481	471	12,467	470	a
NYM-13-86	*Be-10 (qtz)*	*25,587*	*1677*	*25,486*	*1677*	*25,504*	*1678*	P
NYM-13-87	Be-10 (qtz)	13,068	256	13,068	256	13,049	256	a
Snøfonn LG Outermost								
ROD-12-42	*Be-10 (qtz)*	*17,846*	*383*	*17,844*	*383*	*18,141*	*390*	a
ROD-12-43	Be-10 (qtz)	13,250	343	13,220	343	13,424	348	a
ROD-12-44	Be-10 (qtz)	14,284	472	14,188	472	14,408	480	P
ROD-12-45	Be-10 (qtz)	14,958	299	14,898	299	15,134	303	P
Additional Samples								
ROD-12-12	Be-10 (qtz)	11,645	258	11,645	258	11,776	262	a
ROD-12-14	Be-10 (qtz)	13,552	254	13,551	254	13,768	258	a
ROD-12-15	Be-10 (qtz)	11,950	224	11,950	224	12,131	227	a

Table 2 (*continued*)

Sample name	Nuclide	St		Lm		LSDn		
		Age (yr)	error (yr)	Age (yr)	error (yr)	Age (yr)	error (yr)	
ROD-12-17	Be-10 (qtz)	11,247	211	11,237	211	11,396	214	P
ROD-12-24	Be-10 (qtz)	11,560	225	11,510	225	11,663	228	P
ROD-12-29	*Be-10 (qtz)*	*9659*	*251*	*9609*	*251*	*9716*	*254*	P
ROD-12-30	*Be-10 (qtz)*	*11,054*	*236*	*11,014*	*236*	*11,162*	*239*	a
ROD-12-31	*Be-10 (qtz)*	*6296*	*135*	*6296*	*135*	*6404*	*137*	a
ROD-12-32	Be-10 (qtz)	11,933	315	11,932	315	12,076	318	P
ROD-12-33	Be-10 (qtz)	12,364	279	12,364	279	12,519	283	a
ROD-12-54	Be-10 (qtz)	12,091	238	12,091	238	12,213	241	P
ROD-12-SS	*Be-10 (qtz)*	*17,257*	*354*	*17,206*	*354*	*17,405*	*358*	P
ROD-12-62	Be-10 (qtz)	13,296	252	13,296	252	13,439	255	a
ROD-12-63	*Be-10 (qtz)*	*15,845*	*360*	*15,840*	*360*	*16,028*	*364*	a
ROD-12-64	Be-10 (qtz)	13,151	248	13,111	248	13,257	251	P

the intermediate sequence (M5-M10) yield ages within the YD period: YD1 (M7): 12.3 ± 0.8 ka (n = 8; no outlier), YD2 (M9): 12.0 ± 1.0 ka (n = 5, excluding one sample, '-61', as 2σ outlier) and YD3 (M10): 11.5 ± 0.7 ka (n = 8; no outlier, one duplicate: sample 37/84). These moraine ages statistically overlap within 1σ error. However, we note that the chronology of these moraines follows their stratigraphic order (YD1 > YD2 > YD3). The glacier stabilization 12.3 ka ago (YD1/M7) ends a period of glacier retreat (~100 m equilibrium-line-altitude rise) that began about 13 ka ago from the position of moraine M4.

The eight ^{10}Be ages from the 'historic' moraine boulders (M11-M13) also yield ages consistent to the stratigraphic order with LIA1 (M11): 480 ± 20 a (n = 3; no outlier) and LIA2 (M12): 390 ± 100 a (n = 5, excluding sample 68 as 2σ outlier), strengthening the case that mapping and ^{10}Be surface exposure dating together can resolve distinct moraines deposited during the last millennium and the LIA (Schaefer et al., 2009; Schimmelpfennig et al., 2014). Similar LIA moraine sequences have been mapped in numerous glacier forelands in Scandinavia (Nesje et al., 2008).

We present our modeling results in two steps: (i) The results of the ELA lowering for the respective Rødhetta moraines (Supplementary Information)) are given in Table S1; (ii) The changes in precipitation (with constant temperature) and changes in temperature (with constant precipitation) that would drive Rødhetta Glacier to the respective moraine are given in Table S2. The reconstructed precipitation changes for the ELA changes range from ~60% at the LIA to ~165% at the YD. These are large changes in precipitation despite being extremely conservative estimates (see Supplemental Materials for details). In addition, precipitation during Arctic cold periods like the LIA and the YD was most likely reduced by the expanse of sea ice relative to present. On the other hand, our temperature changes reconstructed from the ELA changes for the LIA compare well with the 0.05–0.1 °C/decade warming reported for nearby regions in Scandinavia during the past 100–150 years (Luterbacher et al., 2004). Therefore, glaciers in this regions were likely driven primarily by summer temperature, in accordance with theoretical studies (Anderson et al., 2010; Rupper and Roe, 2008).

The results of the ELA modeling indicate that the LG (M1) ELA lowering of 220 ± 45 m was nearly 100 m lower than the YD ELA that was about 125 ± 40 m lower than the ELA in the sampling year CE 2013 (Fig. 3; Table S2). We estimate that a summer temperature decrease of 1.2–3.2 °C as compared to present (Tables S1 and S2) would advance Rødhetta Glacier to the LG (M1) position. The ~125 m lower ELA during the YD (M7) corresponds to a 0.8–1.9 °C decrease in summer temperature in our model. Finally, the ELA during LIA2 (M12) was 80 ± 20 m lower than present and our glacier model requires about 0.5–0.8 °C summer cooling as compared to present day to reach this moraine. As an independent test of our model-temperature results, we force a dynamic flowline glacier model (Hutter, 1983; Oerlemans et al., 1998; Patankar, 1980; Roe and Baker, 2014), which uses the shallow-ice approximation and parameterized sliding (Farinotti et al., 2009), with these temperature reconstructions. In particular, we model glacier mass balance along the modeled glacier flowlines using the degree-day model for melt and assuming precipitation is equal to present-day. The simulated changes in glacier length match the moraine sequences well (Figs. 3 and S3). The climate reconstructions are consistent for two different modeling approaches (the ELA model and the dynamic glacier model) and our LIA2 reconstruction matches direct observations, suggesting that our first-order climate reconstructions are robust.

5. Discussion

Based on these results, we now present the most likely sequence of glacier events (Fig. 5), reflecting LG summer temperature changes in Arnøya, Arctic Norway: (i) The LG culmination occurred 13.9 ± 0.7 ka ago, and therefore during the Bølling/Allerød period preceding the YD, and was substantially more extensive than the YD glacier advances; (ii) Sustained glacier retreat/summer temperature warming occurred between 13 ka and 12.3 ka, through the first half of the YD stadial; (iii) Glaciers/summer temperatures stabilized at smaller/warmer configuration in mid-YD time followed by modest oscillatory retreat through the rest of the YD; and (iv) no subsequent glacier culminations were identified during the Holocene, presumably reflecting small glaciers and warm summers, until the LIA period. The finding that the LG culmination in Arctic Norway occurred prior to the YD, invigorates the importance of the few pioneering studies reporting the LG culmination moraines of the SIS to be of Older Dryas age (Andersen, 1968; Kverndal and Sollid, 1993).

These LG mountain glacier patterns in Arctic Norway are corroborated by regional glacier records and ^{10}Be chronologies in the Arctic, if calculated consistently (Fig. 5). The ^{10}Be moraine chronologies from the Scorsby Sound region in East Greenland (Kelly et al., 2008; Levy et al., 2016), yield age brackets of 14.3-12.8 ka for the major LG culminations and of 12.9-11.4 ka for the subsequent smaller LG glacier advance. ^{10}Be moraine chronologies of SIS outlet glaciers in western Norway (Briner et al., 2014; Mangerud et al., 2013) yield a similar glacier pattern (Fig. 5). Thus, small Arctic mountain glacier and the mighty Scandinavian Ice Sheet show generally coherent LG pattern of culmination and retreat, a case recently shown for glaciers on Baffin Island and the west Greenland Ice Sheet during the early Holocene (Young et al., 2020).

In an interhemispheric context, several comprehensive ^{10}Be moraine chronologies from New Zealand and Patagonia converge and show the LG culmination during the BA/ACR period (Garcia

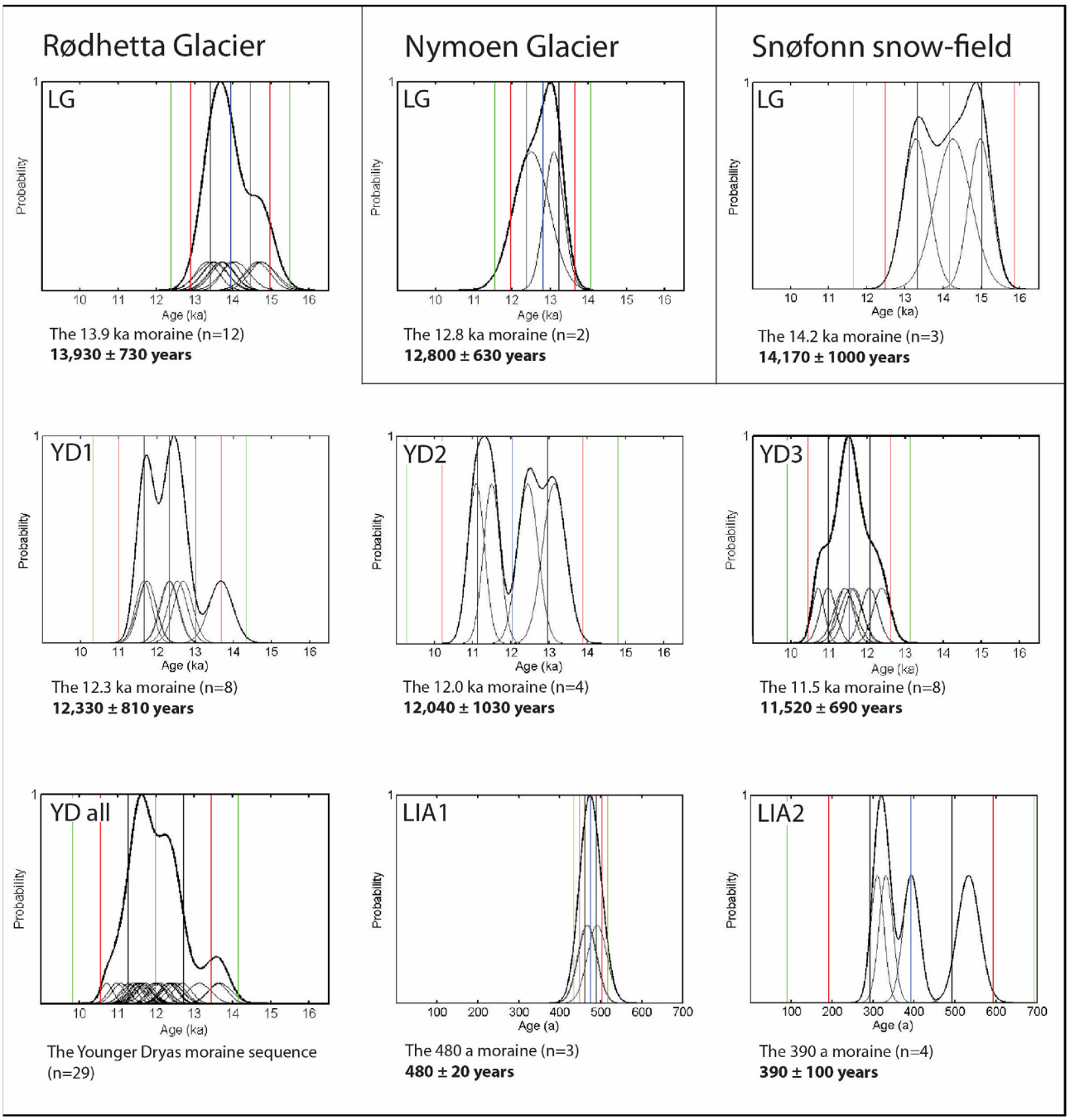

Fig. 4. Probability distribution of ^{10}Be boulder and moraine ages for the moraine ridges of Rødhetta Glacier culminations during the Late Glacial and Holocene periods. The thick black line shows the probability distribution of the ^{10}Be age population, including all individual boulders normalized to 1. Individual ^{10}Be boulder ages within 1σ uncertainties are indicated with thin black lines. The vertical blue line represents the arithmetic mean of all distributions, with a 1σ grey, 2σ red and 3σ green line. For the eventual age of the Rødhetta moraines, we use the arithmetic mean within the standard deviation (1σ) of all individual boulder ages from the respective moraine, including the production rate uncertainty calibrated to 3.7% in (Young et al., 2013). (For interpretation of the references to color in this figure legend, the reader is referred to the Web version of this article.)

et al., 2012; Mendelova et al., 2020; Putnam et al., 2010b; Sagredo et al., 2018) and retreating glaciers through the YD stadial (Kaplan et al., 2010; Sagredo et al., 2018). A similar LG pattern was reported from mountain glaciers in the tropics (Jomelli et al., 2014).

Together, these detailed and robust moraine chronologies support the hypothesis of generally coherent glacier and summer temperature variations on both hemispheres during the LG period, contrasting the traditional view of the bipolar see saw of inter-hemispheric climate (Fig. 5). Hemispheric or regional driving mechanisms, such as the asynchronous northern versus southern solar insolation changes, cannot explain the glacier observations.

However, recent temperature analyses (Buizert et al., 2014) based on different Greenland ice-core δ^{18}O records combined with model simulations, highlight the drastic variation in seasonality (winter-summer temperature difference) (Fig. 5, lowest panel) during the LG, with seasonality extremes during the coldest periods, such as Heinrich Stadial 1 (HS1: 18–14.9 ka ago) and the YD, also referred to as HS0. Summer temperatures show a general

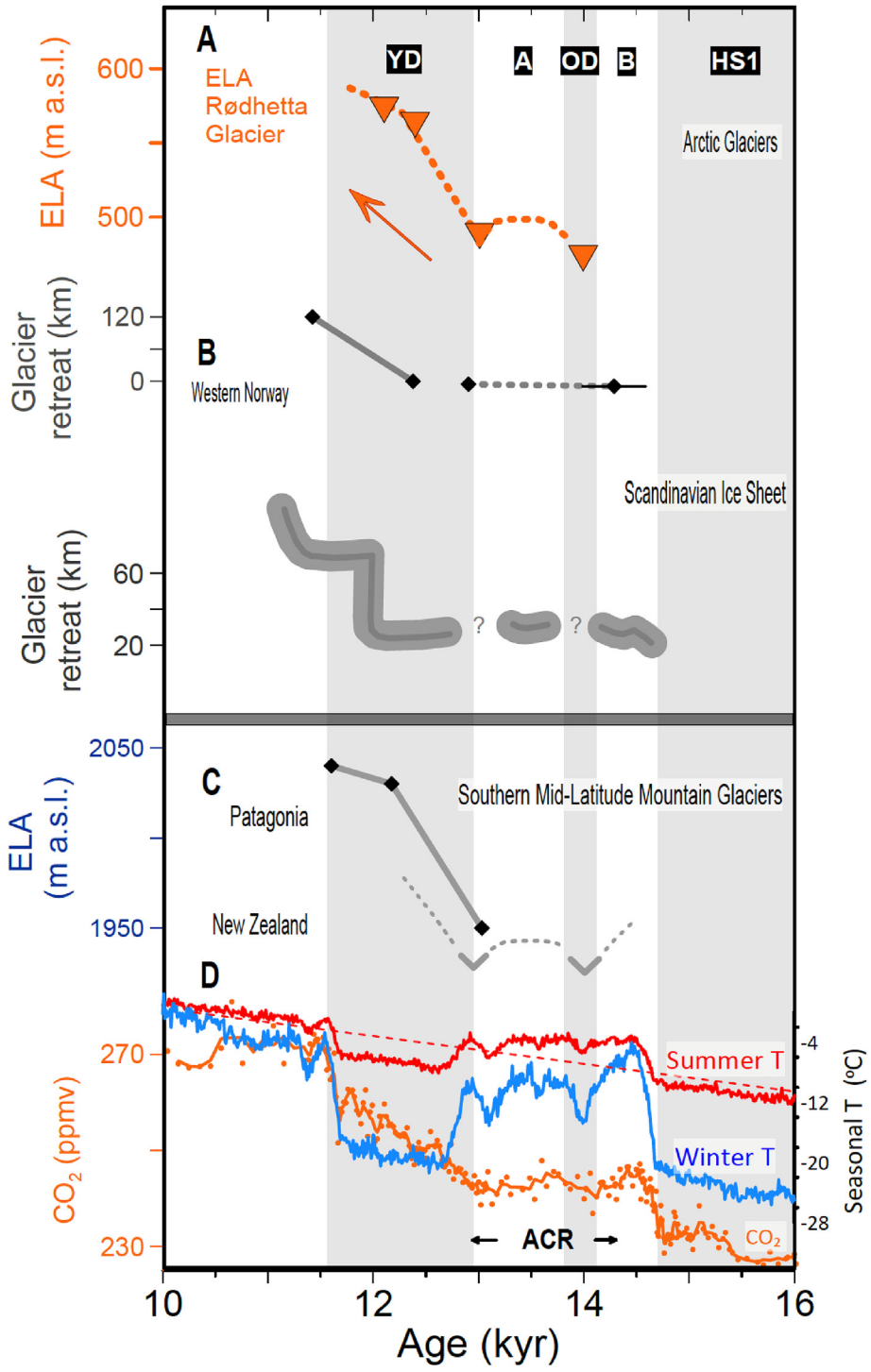

Fig. 5. Rødhetta Glacier changes through the Late Glacial period in a regional and interhemispheric context. Grey and white bars denote the intervals YD=Younger Dryas; A = Allerød; OD=Older Dryas; B=Bølling; ACR = Antarctic Cold Reversal (see text); HS1=Heinrich Stadial 1; A) Rødhetta Glacier, Arctic Norway. Triangles denote glacier culminations/moraine ages plotted against modeled changes in Equilibrium Line Altitude. The arrow denotes the glacier retreat through the YD period. B) Recent ^{10}Be chronologies of the SIS in western Norway (Briner et al., 2014; Mangerud et al., 2013) re-calculated consistently with the Arctic Production Rate (Young et al., 2013) (lower graph) and a ^{14}C chronology of the SIS at Langnes in Troms County (upper graph) (Andersen, 1968), indicating a quasi-stable western and Arctic SIS during the BA/ACR followed by retreat through the YD stadial. C) Glacier evolution in the southern mid-latitudes based on records from New Zealand's Southern Alps (Kaplan et al., 2010; Koffman et al., 2017; Putnam et al., 2010b) and Patagonia (Garcia et al., 2012; Sagredo et al., 2018; Strelin et al., 2011), showing a consistent picture of glacier culminations during the ACR and subsequent glacier retreat/summer temperature warming during the YD stadial. D) Atmospheric CO_2 concentration (orange) (Monnin et al., 2001) and seasonal Greenland temperatures derived from models and Greenland ice core water isotope data (modified from Buizert et al. (2018)). (For interpretation of the references to color in this figure legend, the reader is referred to the Web version of this article.)

warming trend over the LG, including a warming through the YD (Alley, 2000), with superimposed subdued abrupt climate changes of only a few °C from HS1 to the Bølling, from Allerød into the YD, and from YD to the Holocene. These Greenland-summer temperature patterns show consistency with the mountain glacier patterns presented here and are also roughly similar to Antarctic mean annual temperature and atmospheric CO_2 records, potentially explaining the inter-hemispherically coherent pattern of summer temperature sensitive mountain glaciers changes during the LG. If correct, this would mean that the inter-hemispheric bipolar seesaw is not prominent during northern summers, and mostly a North Atlantic winter phenomenon during cold periods, masking the inter-hemispheric summer warming reflected by mountain glaciers around the globe. This scenario can be tested by more such detailed glacier studies of Northern Hemisphere moraine records through the LG period, and, in turn, precise ^{10}Be chronologies of key moraine records throughout Scandinavia, the Alps and the Western US, among others, hold the key to verify or falsify this concept of the seasonality-switch of the bipolar see saw that would alter our basic understanding of inter-hemispheric climate.

Author statement

HEW conducted field-work, processes samples, analyzed data and wrote first draft. JMS super-vised HEW during laboratory work, analyzed the data and their climate relevance, and actively participated in writing the final manuscript. JB was main supervisor of HEW's PhD, supervised the field work, participated in the data analyses and writing of the paper. SBR lead the glacier modeling aspect of this manuscript, contributed to the paleoclimate analyses of the data and model results and lead the writing of the modeling manuscript sections. OP assisted in the field work, and contributed to the writing of this manuscript. RS trained and supervised HEW during the rock processing for ^{10}Be chemistry in the laboratory. RCF was responsible for the high quality of the Accelerator Mass Spectrometry beryllium isotope measurements, contributed to the data analyses and the writing of this paper.

Declaration of competing interest

The authors declare that they have no know competing financial interests or personal relationships that could have appeared to influence the work reported in this paper.

Acknowledgements

We thank J. Hanley and K. Needleman for help with sample preparation, H. and A. Wittmeier and S. Ludwig for field assistance, and E. and J. Johannessen at Lauksletta Overnatting for accommodation. This study was funded by the Norwegian Research Council, Norway (Project SHIFTS, University of Bergen), the Columbia Climate Center, the G. Unger Vetlesen Foundation and the Lamont-Doherty Earth Observatory. This is LDEO publication #8428.

Appendix A. Supplementary data

Supplementary data to this article can be found online at https://doi.org/10.1016/j.quascirev.2020.106461.

References

Aarseth, I., Mangerud, J., 1974. Younger Dryas end moraines between Hardangerfjorden and Sognefjorden, western Norway. Boreas 3, 3–22.
Alley, R.B., 2000. The Younger Dryas cold interval as viewed from central Greenland. Quat. Sci. Rev. 19, 213–226.
Andersen, B.G., Mangerud, J., Sørensen, R., Reite, A., Sveian, H., Thoresen, M., Bergstrøm, B., 1995. Younger Dryas ice-marginal deposits in Norway. Quat. Int. 28, 147–169.
Andersen, B.J., 1968. Glacial Geology of Western Troms, North Norway. Universitetsforlaget, Oslo, Norges geologiske undersøkelse (Series), nr. 256, p. 160.
Anderson, B., Mackintosh, A., Stumm, D., George, L., Kerr, T., Winter-Billington, A., Fitzsimons, S., 2010. Climate sensitivity of a high-precipitation glacier in New Zealand. J. Glaciol. 56, 114–128.
Andreassen, K., Vorren, T., Johansen, K., 1985. Pre-Late Weichselian glacimarine sediments at Arnøy, north Norway. Geol. Foren. Stockh. Forh. 107, 63–70. https://doi.org/10.1080/11035898509452615.
Bakke, J., Dahl, S.O., Paasche, O., Lovlie, R., Nesje, A., 2005. Glacier fluctuations, equilibrium-line altitudes and palaeoclimate in Lyngen, northern Norway, during the Lateglacial and Holocene. Holocene 15, 518–540.
Balco, G., Briner, J.P., Rayburn, J., Ridge, J.C., Schaefer, J.M., 2009. Regional beryllium-10 production rate calibration for northeastern North America. Quat. Geochronol. 4, 93–107.
Benn, D., Evans, D.J., 2014. Glaciers and Glaciation, 2 ed. Routledge, p. 802.
Braithwaite, R., Zhang, Y., 2000. Sensitivity of mass balance of five Swiss glaciers to temperature changes assessed by tuning a degree-day model. J. Glaciol. 46, 7–14.
Briner, J.P., Svendsen, J.I., Manferud, J., Lohne, Ø.S., Young, N.E., 2014. A 10Be chronology of south-western Scandinavian Ice Sheet history during the Lateglacial period. J. Quat. Sci. 29, 370–380.
Broecker, W.S., 1998. Paleocean circulation during the last deglaciation: a bipolar seesaw? Paleoceanography 13, 119–121.
Bromley, G.R., Putnam, A.E., Rademaker, K.M., Lowell, T.V., Schaefer, J.M., Hall, B., Winckler, G., Birkel, S.D., Borns, H.W., 2014. Younger Dryas deglaciation of Scotland driven by warming summers. Proc. Natl. Acad. Sci. Unit. States Am. 111, 6215–6219.
Buizert, C., Gkinis, V., Severinghaus, J.P., He, F., Lecavalier, B.S., Kindler, P., Leuenberger, M., Carlson, A.E., Vinther, B., Masson-Delmotte, V., White, J.W.C., Liu, Z., Otto-Bliesner, B., Brook, E.J., 2014. Greenland temperature response to climate forcing during the last deglaciation. Science 345, 1177–1180. https://doi.org/10.1126/science.1254961.
Buizert, C., Keisling, B.A., Box, J.E., He, F., Carlson, A.E., Sinclair, G., DeConto, R.M., 2018. Greenland-wide seasonal temperatures during the last deglaciation. Geophys. Res. Lett. 45, 1905–1914. https://doi.org/10.1002/2017gl075601.
Claude, A., Ivy-Ochs, S., Kober, F., Antognini, M., Salcher, B., Kubik, P., 2014. The Chironico landslide (Valle Leventina, southern Swiss Alps): age and evolution. Swiss J. Geosci. https://doi.org/10.1007/s00015-014-0170-z.
Cuffey, K.M., Paterson, W.S.B., 2010. The Physics of Glaciers. Academic Press, p. 704.
Evans, D.J., Rea, B.R., Hansom, J.D., Whalley, W.B., 2002. Geomorphology and style of plateau icefield deglaciation in fjord terrains: the example of Troms-Finnmark, north Norway. J. Quat. Sci. 17, 221–239.
Farinotti, D., Huss, M., Bauder, A., Funk, M., Truffer, M., 2009. A method to estimate the ice volume and ice-thickness distribution of alpine glaciers. J. Glaciol. 55, 422–430.
Fenton, C.R., Hermanns, R.L., Blikra, L.H., Kubik, P.W., Bryant, C., Niedermann, S., Meixner, A., Goethals, M.M., 2011. Regional (10)Be production rate calibration for the past 12 ka deduced from the radiocarbon-dated Grotlandsura and Russenes rock avalanches at 69 degrees N, Norway. Quat. Geochronol. 6, 437–452. https://doi.org/10.1016/j.quageo.2011.04.005.
Garcia, J.L., Kaplan, M.R., Hall, B.L., Schaefer, J.M., Vega, R.M., Schwartz, R., Finkel, R., 2012. Glacier expansion in southern Patagonia throughout the Antarctic cold reversal. Geology 40, 859–862. https://doi.org/10.1130/g33164.1.
Goehring, B.M., Lohne, O.S., Mangerud, J., Svendsen, J.I., Gyllencreutz, R., Schaefer, J., Finkel, R., 2012. Late glacial and holocene ^{10}Be production rates for western Norway. J. Quat. Sci. 27, 89–96. https://doi.org/10.1002/jqs.1517.
Harris, I., Jones, P., Osborn, T., Lister, D., 20. Updated high-resolution grids of monthly climatic observations–the CRU TS3. 10 Dataset. Int. J. Climatol. 34, 623–642€.
Hock, R., 2003. Temperature index melt modelling in mountain areas. J. Hydrol. (NZ) 282, 104–115.
Hutter, K., 1983. Theoretical Glaciology: Material Science of Ice and the Mechanics of Glaciers and Ice Sheets. Springer Netherlands, Mathematical Approaches to Geophysics, p. 510.
Ivy-Ochs, S., Kerschner, H., Maisch, M., Christl, M., Kubik, P.W., Schlüchter, C., 2009. Latest pleistocene and holocene glacier variations in the European Alps. Quat. Sci. Rev. 28, 2137–2149.
Jomelli, V., Favier, V., Vuille, M., Braucher, R., Martin, L., Blard, P.H., Colose, C., Brunstein, D., He, F., Khodri, M., Bourles, D.L., Leanni, L., Rinterknecht, V., Grancher, D., Francou, B., Ceballos, J.L., Fonseca, H., Liu, Z., Otto-Bliesner, B.L., 2014. A major advance of tropical Andean glaciers during the Antarctic cold reversal. Nature 513, 224–227.
Kaplan, M.R., Schaefer, J.M., Denton, G.H., Barrell, D.J., Chinn, T.J., Putnam, A.E., Andersen, B.G., Finkel, R.C., Schwartz, R., Doughty, A.M., 2010. glacier retreat in New Zealand during the younger Dryas stadial. Nature 467, 194–197.
Kaplan, M.R., Strelin, J.A., Schaefer, J.M., Denton, G.H., Finkel, R.C., Schwartz, R., Putnam, A.E., Vandergoes, M.J., Goehring, B.M., Travis, S.G., 2011. In-situ cosmogenic (10)Be production rate at Lago Argentino, Patagonia: implications for late-glacial climate chronology. Earth Planet Sci. Lett. 309, 21–32.
Kelly, M.A., Lowell, T.V., Hall, B.L., Schaefer, J.M., Finkel, R.C., Goehring, B.M., Alley, R.B., Denton, G.H., 2008. A ^{10}Be chronology of lateglacial and Holocene mountain glaciation in the Scoresby Sund region, east Greenland: implications for seasonality during lateglacial time. Quat. Sci. Rev. 27, 2273–2282.

Koffman, T.N., Schaefer, J.M., Putnam, A.E., Denton, G.H., Barrell, D.J., Rowan, A.V., Finkel, R.C., Rood, D.H., Schwartz, R., Plummer, M.A., 2017. A beryllium-10 chronology of late-glacial moraines in the upper Rakaia valley, Southern Alps, New Zealand supports Southern-Hemisphere warming during the Younger Dryas. Quat. Sci. Rev. 170, 14–25.

Kverndal, A.-I., Sollid, J.L., 1993. Late Weichselian glaciation and deglaciation in northeastern Troms, northern Norway. Nor. J. Geogr. 47, 163–177.

Lal, D., 1991. Cosmic ray labeling of erosion surfaces: in situ nuclide production rates and erosion models. Earth Planet Sci. Lett. 104, 424–439.

Levy, L.B., Kelly, M.A., Lowell, T.V., Hall, B.L., Howley, J.A., Smith, C.A., 2016. Coeval fluctuations of the Greenland ice sheet and a local glacier, central East Greenland, during late glacial and early Holocene time. Geophys. Res. Lett. 43, 1623–1631. https://doi.org/10.1002/2015gl067108.

Luterbacher, J., Dietrich, D., Xoplaki, E., Grosjean, M., Wanner, H., 2004. European seasonal and annual temperature variability, trends, and extremes since 1500. Science 303, 1499–1503.

Lüthi, M., 2014. Little Ice Age climate reconstruction from ensemble reanalysis of Alpine glacier fluctuations. Cryosphere 8, 639–650.

Mangerud, J., Goehring, B.M., Lohne, O.S., Svendsen, J.I., Gyllencreutz, R., 2013. Collapse of marine-based outlet glaciers from the Scandinavian ice sheet. Quat. Sci. Rev. 67, 8–16. https://doi.org/10.1016/j.quascirev.2013.01.024.

Mendelova, M., Hein, A.S., Rodes, A., Smedley, R.K., Xu, S., 2020. Glacier expansion in central Patagonia during the Antarctic cold reversal followed by retreat and stabilisation during the younger Dryas. Quat. Sci. Rev. 227 https://doi.org/10.1016/j.quascirev.2019.106047.

Mitchell, T.D., Carter, T.R., Jones, P.D., Hulme, M., New, M., 2004. A Comprehensive Set of High-Resolution Grids of Monthly Climate for Europe and the Globe: The Observed Record (1901–2000) and 16 Scenarios (2001–2100). Tyndall Centre for Climate Change Research Working Paper 55, p. 25.

Møller, J., Sollid, J., 1972. Deglaciation chronology of Lofoten–Vesterålen–Ofoten, north Norway. Nor. J. Geogr. 26, 101–133.

Monnin, E., Indermuehle, A., Daellenbach, A., Flueckiger, J., Stauffer, B., Stocker, T.F., Raynaud, D., Barnola, J.-M., 2001. Atmospheric CO_2 concentrations over the last glacial termination. Science 291, 112–114.

Nesje, A., Bakke, J., Dahl, S.O., Lie, Ø., Matthews, J.A., 2008. Norwegian mountain glaciers in the past, present and future. Global Planet. Change 60, 10–27.

Nishiizumi, K., Imamura, M., Caffee, M.W., Southon, J.R., Finkel, R.C., McAninch, J., 2007. Absolute calibration of ^{10}Be AMS standards. Nucl. Instrum. Methods Phys. Res. B 258, 403–413.

Oerlemans, J., 2001. Glaciers and Climate Change. A.A. Balkema Publishers, Rotterdam, p. 148.

Oerlemans, J., 2005. Extracting a climate signal from 169 glacier records. Science 308, 675–677.

Oerlemans, J., Anderson, B., Hubbard, A., Huybrechts, P., Johannesson, T., Knap, W., Schmeits, M., Stroeven, A., Van de Wal, R., Wallinga, J., 1998. Modelling the response of glaciers to climate warming. Clim. Dynam. 14, 267–274.

Paasche, Ø., Dahl, S.O., Bakke, J., Lovlie, R., Nesje, A., 2007. Cirque glacier activity in arctic Norway during the last deglaciation. Quat. Res. 68, 387–399.

Patankar, S., 1980. Numerical Heat Transfer and Fluid Flow, vol. 214. CRC Press - Taylor & Francis, Boca Raton. Computational Methods in Mechanics & Thermal Sciences.

Porter, S.C., 1975. Equilibrium-line altitudes of late quaternary glaciers in the southern Alps, New Zealand. Quat. Res. 5, 27–47.

Putnam, A., Schaefer, J., Barrell, D., Vandergoes, M., Denton, G., Kaplan, M., Finkel, R., Schwartz, R., Goehring, B., Kelley, S., 2010a. In situ cosmogenic ^{10}Be production-rate calibration from the Southern Alps, New Zealand. Quat. Geochronol. 5, 392–409.

Putnam, A.E., Bromley, G.R.M., Rademaker, K., Schaefer, J.M., 2019. In situ Be-10 production-rate calibration from a C-14-dated late-glacial moraine belt in Rannoch Moor, central Scottish Highlands. Quat. Geochronol. 50, 109–125.

Putnam, A.E., Denton, G.H., Schaefer, J.M., Barrell, D., Andersen, B.G., Finkel, R., Schwartz, R., Doughty, A.M., Kaplan, M.R., Schlüchter, C., 2010b. glacier advance in southern middle-latitudes during the Antarctic cold reversal. Nat. Geosci. 3, 700–704.

Rasmussen, S.O., Andersen, K.K., Svensson, A., Steffensen, J.P., Vinther, B.M., Clausen, H.B., Siggaard-Andersen, M.L., Johnsen, S.J., Larsen, L.B., Dahl-Jensen, D., 2006. A new Greenland ice core chronology for the last glacial termination. J. Geophys. Res.: Atmos. 111, 1984–2012.

Rasmussen, L., Andreassen, L., 2005. Seasonal mass-balance gradients in Norway. J. Glaciol. 51, 601–606.

Roberts, D., 1973. Hammerfest. Bedrock Map Hammerfest M 1:250 000, Norway Geological Survey - Reports, Trondheim. https://www.ngu.no/publikasjon/hammerfest-berggrunnskart-hammerfest-m-1250-000.

Roe, G.H., Baker, M.B., 2014. Glacier response to climate perturbations: an accurate linear geometric model. J. Glaciol. 60, 670–684.

Romundset, A., Bondevik, S., Bennike, O., 2011. Postglacial uplift and relative sea level changes in Finnmark, northern Norway. Quat. Sci. Rev. 30, 2398–2421.

Rupper, S., Roe, G., 2008. glacier changes and regional climate: a mass and energy balance approach. J. Clim. 21, 5384–5401.

Sagredo, E.A., Kaplan, M.R., Araya, P.S., Lowell, T.V., Aravena, J.C., Moreno, P.I., Kelly, M.A., Schaefer, J.M., 2018. Trans-pacific glacial response to the Antarctic Cold Reversal in the southern mid-latitudes. Quat. Sci. Rev. 188, 160–166.

Schaefer, J.M., Denton, G.H., Kaplan, M., Putnam, A., Finkel, R.C., Barrell, D.J., Andersen, B.G., Schwartz, R., Mackintosh, A., Chinn, T., 2009. High-frequency Holocene glacier fluctuations in New Zealand differ from the northern signature. Science 324, 622–625.

Schimmelpfennig, I., Schaefer, J.M., Akcar, N., Koffman, T., Ivy-Ochs, S., Schwartz, R., Finkel, R.C., Zimmerman, S., Schluechter, C., 2014. A chronology of Holocene and Little Ice Age glacier culminations of the Steingletscher, Central Alps, Switzerland, based on high-sensitivity beryllium-10 moraine dating. Earth Planet Sci. Lett. 393, 220–230. https://doi.org/10.1016/j.epsl.2014.02.046.

Six, D., Vincent, C., 2014. Sensitivity of mass balance and equilibrium-line altitude to climate change in the French Alps. J. Glaciol. 60, 867–878.

Sollid, J., Andersen, S., Hamre, N., Kjeldsen, O., Salvigsen, O., Sturød, S., Tveitå, T., Wilhelmsen, A., 1973. Deglaciation of Finnmark, north Norway. Nor. J. Geogr. 27, 233–325.

Staiger, J., Gosse, J., Toracinta, R., Oglesby, B., Fastook, J., Johnson, J.V., 2007. Atmospheric scaling of cosmogenic nuclide production: climate effect. J. Geophys. Res.: Solid Earth 112. https://doi.org/10.1029/2005jb003811.

Stokes, C.R., Corner, G.D., Winsborrow, M.C., Husum, K., Andreassen, K., 2014. Asynchronous response of marine-terminating outlet glaciers during deglaciation of the Fennoscandian Ice Sheet. Geology 42, 455–458.

Stone, J., 2000. Air pressure and cosmogenic isotope production. J. Geophys. Res. 105, 23753–23759.

Strelin, J.A., Denton, G.H., Vandergoes, M.J., Ninnemann, U.S., Putnam, A.E., 2011. Radiocarbon chronology of the late-glacial Puerto Bandera moraines, southern Patagonian icefield, Argentina. Quat. Sci. Rev. 30, 2551–2569.

Thibert, E., Eckert, N., Vincent, C., 2013. Climatic drivers of seasonal glacier mass balances: an analysis of 6 decades at Glacier de Sarennes (French Alps). Cryosphere 7, 47–66.

Vincent, C., Vallon, M., 1997. Meteorological controls on glacier mass balance: empirical relations suggested by measurements on glacier de Sarennes, France. J. Glaciol. 43, 131–137.

Wittmeier, H.E., Bakke, J., Vasskog, K., Trachsel, M., 2015. Reconstructing Holocene glacier activity at Langfjordjokelen, Arctic Norway, using multi-proxy fingerprinting of distal glacier-fed lake sediments. Quat. Sci. Rev. 114, 78–99. https://doi.org/10.1016/j.quascirev.2015.02.007.

Young, N.E., Briner, J.P., Miller, G.H., Lesnek, A.J., Crump, S.E., Thomas, E.K., Pendleton, S.L., Cuzzone, J., Lamp, J., Zimmerman, S., Caffee, M., Schaefer, J.M., 2020. Deglaciation of the Greenland and Laurentide ice sheets interrupted by glacier advance during abrupt coolings. Quat. Sci. Rev. 229, 106091.

Young, N.E., Schaefer, J.M., Briner, J.P., Goehring, B.M., 2013. A Be-10 production-rate calibration for the Arctic. J. Quat. Sci. 28, 515–526.